Domain Organization and Quaternary Structure of the *Saccharomyces cerevisiae* Silent Information Regulator 3 Protein, Sir3p

Steven J. McBryant, Christine Krause, and Jeffrey C. Hansen*

Department of Biochemistry and Molecular Biology, Colorado State University, Fort Collins, Colorado 80523-1870

Received August 18, 2006; Revised Manuscript Received October 13, 2006

ABSTRACT: The silent information regulator protein 3 (Sir3p) functions in the initiation, propagation, and maintenance of transcriptionally silenced chromatin in *Saccharomyces cerevisiae*. To better understand the physicochemical basis for its effects on chromatin architecture, recombinant full-length *S. cerevisiae* Sir3p has been purified to near homogeneity on the large-scale and characterized by circular dichroism, limited protease digestion, and analytical ultracentrifugation. Results indicate that the Sir3p monomer has a unique tripartite domain organization, including a nearly 300-amino-acid residue stretch of intrinsically disordered residues that lies internal to its structured N- and C-terminal regions. Sir3p self-associates extensively in moderate salt and at micromolar protein concentrations producing a broad range of oligomers that sediment from 8 to in excess of 85 S. These results provide new insight into Sir3p domain organization and quaternary structure and support a nucleosome bridging model for Sir3p-dependent regulation of chromatin architecture.

The budding yeast *Saccharomyces cerevisiae* lacks the classical heterochromatin components found in higher organisms. Instead, it assembles a unique repressive nucleoprotein structure termed "silenced chromatin", which is found at telomeres and at a region of chromosome 3 containing the silent mating type loci, *HML* and *HMR* (*1*). Silenced chromatin is initiated and maintained by the silent information regulator (SIR) proteins, Sir1p, Sir2p, Sir3p, and Sir4p. Assembly of silent chromatin begins when the origin recognition complex (ORC)[1] binds to specific cis-acting silencer DNA elements. Sir1p subsequently binds to the ORC−DNA complex (*2*−*4*) and recruits the other SIRs to form a SIR protein complex (*5*−*9*). After initiation, Sir2p, Sir3p, and Sir4p "spread" away from the silencer element to establish and maintain transcriptionally repressed chromosomal domains. Silenced genomic regions in *S. cerevisiae* encompass between 0.2 and 8 kbp of DNA, indicating that silencing occurs at both the local and the global levels (*10*−*12*).

Each of the SIR proteins function uniquely in silencing. Sir1p can initiate assembly of silencing in the absence of ORC or Rap1 (*2*, *13*, *14*) and is not required for spreading of silenced chromatin (*15*, *16*), suggesting that it functions to recruit other SIR proteins during initiation. Sir4p appears to provide a platform for assembling SIR complexes in chromatin, as it contains binding sites for Sir1p, Sir2p, Sir3p, Rap1, and the histone H3 and H4 NTDs (*8*, *15*, *17*). Sir2p is a NAD-dependent histone deacetylase that catalyzes deacetylation of lysine 9 and 14 of the histone H3 NTD and lysine 16 of the H4 NTD (*5*, *18*, *19*). The histone deacetylase function of Sir2p is not required to initiate silencing (*8*, *15*) but helps maintain silent chromatin by keeping the histone H3 and H4 NTDs in the hypoacetylated form that preferentially recruits Sir3p (*5*, *20*, *21*). Sir3p appears to function as a chromatin architectural protein (*22*, *23*), as overexpression of Sir3p in vivo leads to "spreading" of silenced chromatin into previously euchromatic regions. Moreover, the levels of Sir2p and Sir4p in this newly silenced chromatin are diminished relative to Sir3p (*24*−*26*). Thus, Sir3p−chromatin interactions appear to be sufficient to maintain transcriptionally silent chromatin. On the basis of these results, a model for silenced telomeric chromatin has been proposed in which islands of "core" silent chromatin containing all three SIRs and Rap1 are interspersed among chromosomal regions that contained primarily Sir3p (*26*).

Consistent with its architectural function in vivo, Sir3p binds to nucleosomal arrays in vitro and assembles them into higher order secondary and tertiary chromatin structures (*22*, McBryant et al., manuscript in preparation). Sir3p has been proposed to mediate its effects on chromatin structure through a nucleosome "bridging" mechanism, in which simultaneous interaction with nearby nucleosomes leads to local changes in chromatin structure, while interactions with widely separated nucleosomes cause global structural changes (*23*). A key tenet of this model is that Sir3p is oligomeric when bound to chromatin, and thus each Sir3p particle will possess multiple chromatin binding sites. Similarly, Sir3p oligomerization also may contribute to the mechanism of silent chromatin spreading. However, largely because of the inability to purify the protein on the large scale, there has been no systematic physicochemical characterization of full-length Sir3p in solution. Here we describe the purification of milligram quantities of full-length recombinant Sir3p to ≥95% homogeneity from sf-9 cells. Circular dichroism (CD) studies demonstrate that nearly one-third of the protein sequence is disordered. Protease mapping and FoldIndex

* Corresponding author. E-mail: jeffrey.c.hansen@colostate.edu. Phone: 970-491-5440. Fax: 970-491-0494.

[1] Abbreviations: CD, circular dichroism; ORC, origin recognition complex; Sir, Silent information regulator.

10.1021/bi061693k CCC: $33.50
Published on Web 12/05/2006

predictions localize most of the disorder to a long internal domain that lies between the structured N- and C-terminal regions. Analytical ultracentrifugation studies have defined the hydrodynamic properties of the Sir3p monomer and show that Sir3p simultaneously populates a wide range of oligomeric states in native solutions. These results provide insight into Sir3p domain organization and quaternary structure and provide a mechanistic framework for understanding how Sir3p influences the architecture of silent chromosomal domains.

MATERIALS AND METHODS

Sir3p Purification. Cultured Sf9 insect cells were infected with a baculovirus vector that expresses recombinant Sir3p fused to six C-terminal histidines (*22*). After infection for 96 h, the cells were lysed by the addition of hypotonic buffer containing 20 mM Tris pH 8.0, 5 mM NaCl, 0.1 mM β-mercaptoethanol, 0.5 mM benzamidine hydrochloride, 0.5 mM PMSF and Dounce homogenization (loose pestle). This and all subsequent steps were carried out on ice or at 4 °C to minimize proteolytic degradation of Sir3p during purification. Cell nuclei were pelleted by differential centrifugation, the supernatant decanted, and the nuclei lysed by resuspension in buffer containing 20 mM Tris pH 8.0, 250 mM NaCl, 0.5 mM β-mercaptoethanol, 1.0 mM benzamidine hydrochloride, 1.0 mM PMSF, 0.01% (v/v) Protease Inhibitor Cocktail Set III (Calbiochem), followed by homogenization in a dounce homogenizer (tight pestle). Lysed nuclei were incubated at 4 °C for 30 min. Ammonium sulfate was added to a final concentration of 10% (w/v). The sample was rotated slowly for 30 min and centrifuged at 31 000 rpm in a Beckman Ti-50.2 rotor for 60 min at 5 °C. The pellet was discarded. Saturated ammonium sulfate was slowly added to the supernatant to a final concentration of 45% (w/v), and the solution was stirred on ice for 30 min. The precipitated Sir3p was pelleted by centrifugation at 20000*g* at 4 °C for 10 min. The Sir3p pellet was resuspended in Buffer A (20 mM Tris pH 8.0, 5% glycerol (v/v), 0.005% nonidet P-40, 0.5 mM β-mercaptoethanol, 0.2 mM benzamidine hydrochloride, 0.5 mM PMSF, 0.01% (v/v) Protease Inhibitor Cocktail Set III (Calbiochem)), and the residual salt concentration was determined by measurement of the solution conductivity. The salt concentration was adjusted to 150 mM by the addition of Buffer A, filtered to 0.45 micron with a syringe-end filter, and applied to a 14 mL Q-Sepharose FF column (GE Healthcare). The column was washed extensively with Buffer A containing 150 mM NaCl, and the bound Sir3p was eluted with a linear NaCl gradient. The Sir3p peak eluted at approximately 325 mM NaCl as determined by SDS−PAGE of the column fractions. Peak fractions were pooled, and the conductivity was adjusted to ~150 mM NaCl by dilution with Buffer A. The sample was applied to a 5 mL Hi-Trap Heparin HP column (GE Healthcare) and eluted with a linear NaCl gradient. The Sir3p peak generally eluted at approximately 550 mM NaCl. Peak fractions were pooled, the NaCl was adjusted to 150 mM by dilution with Buffer A. The sample was applied to a 1 mL Mono-Q (GE Healthcare) column and eluted with a linear salt gradient. The Sir3p peak generally eluted at approximately 400 mM NaCl. The peak fractions were pooled and dialyzed into the desired buffer (see below). The resulting protein was >95% pure as judged by SDS−PAGE (see Figure 1). The extinction coefficient used for protein concentration determination was 83 835 M^{-1} cm^{-1} at 276 nm (ProtParam). This protocol generally yielded 2−5 mg of pure Sir3p from 4 to 8 × 10^3 cm^2 of adherent, infected *Sf*-9 cells.

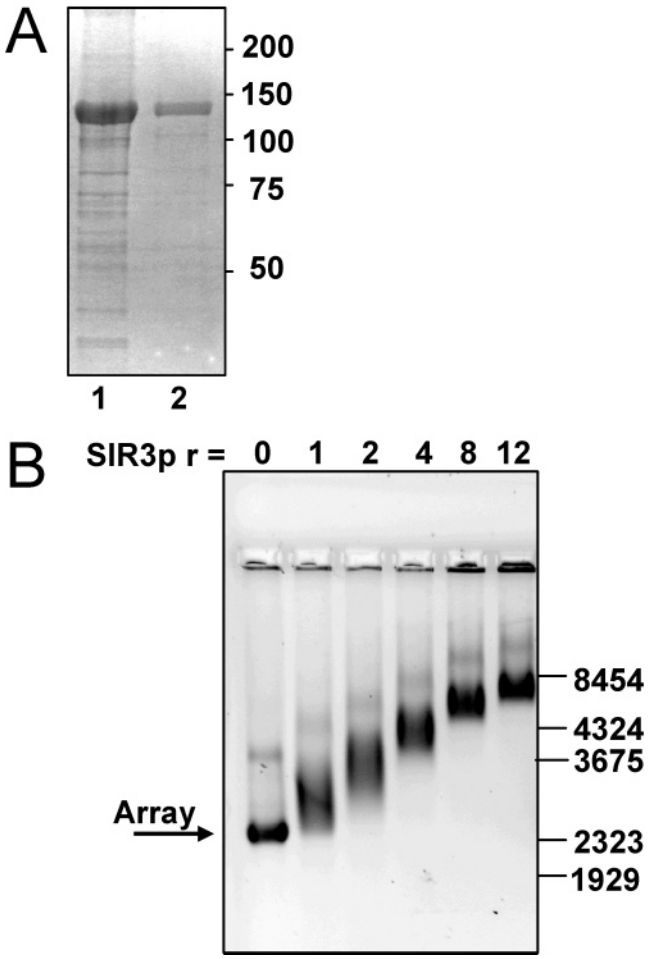

FIGURE 1: Electrophoretic analysis of Sir3p: (A) SDS−PAGE of purified, recombinant SIR3 protein. 10 and 1 μg (lanes 1 and 2, respectively) of Sir3p was separated on a 10% gel and stained with Coomassie Brilliant Blue. The positions of the molecular weight markers are shown at right. (B) 0.5 μg of reconstituted 208−12 nucleosome arrays (3.6 pmol) was incubated with the indicated molar ratio of Sir3p (per 208 bp repeat) in TEN (20 μL reaction volume) prior to electrophoresis on a 1% TAE agarose gel at 5 V/cm for 2 h. The gel was stained with ethidium bromide and visualized by UV trans-illumination. The arrow indicates the position of the unbound nucleosome array, and the positions of bands from a λ-BstEII digest are shown at right. The faint slower migrating band represents dimeric nucleosomal arrays formed during salt dialysis reconstitution.

Electrophoretic Mobility Shift Assay. Defined nucleosomal arrays were assembled from chicken erythrocyte core histone octamers and 208−12 DNA and as described (*27*). Purified Sir3p was mixed with nucleosomal arrays at the indicated molar ratios for 15 min at room temperature. Glycerol was added to a final concentration of 5% (v/v), and the samples were loaded onto a 1% agarose gel buffered with 1× TAE. Gels were electrophoresed at 5 V/cm for 2.5 h at room temperature. The gels were stained with ethidium bromide, visualized using a UV trans-illuminator, and an inverted image recorded using a Gel Logic 200 (Kodak). A Bst EII digest of λ DNA (New England Bio-labs) was used for molecular weight markers.

Circular Dichroism and Intrinsic Disorder Prediction. CD spectroscopy was performed on a Jasco-720 spectropolarimeter at 20 °C. A total of 20 spectra were obtained and averaged to obtain the final spectra. The molar ellipticity [Θ] was obtained by normalization of the measured ellipticity (Θ, mdeg), using [Θ] = (Θ *100)/(*nlc*), where *n* is the number of residues (984), *c* is the total concentration (mM), and *l* is the cell path length (cm). Measurements of Sir3p (1 μM) in the presence of 0.5 M NaCl and guanidine hydrochloride (GuHCl) were only extended to 200−210 nm due to the strong far-UV signal of these solutes. The percentages of specific secondary structure types were determined from the spectra using the CONTINLL, SELCON3, and CDSSTR methods within CDPro analytical software (*28*). Secondary structure predictions were accessed though the ExPASy proteomics tools at http://us.expasy.org/tools/#secondary. FoldIndex plots for predicting intrinsic protein disorder and domain signatures (*29*) were created using a program accessed through the FoldIndex website at http://bioportal.weizmann.ac.il/fldbin/findex#info. The window and step size were set to 6 and 1, respectively.

Analytical Ultracentrifugation. Sedimentation velocity experiments were performed in a Beckman XL-series analytical ultracentrifuge using the absorbance optical system. Samples were loaded into two-sector, charcoal-filled Epon centerpiece assembled with quartz windows and centrifuged in an AN60Ti 4-hole rotor at 21 °C. Velocity data were edited and analyzed using the boundary analysis method of Demeler and van Holde and Weischet to generate G(s) plots (*30*), as implemented in Ultrascan version 7.1. Complementary *c*(*S*) analyses were performed within Sedfit (*31*). Sedimentation coefficients (*s*) are reported in units of Svedbergs (S), where $1\ S = 1 \times 10^{-13}$ s, and were corrected to that of water at 20° ($s_{20,w}$). Modeling of hydrodynamic parameters was performed using Ultrascan. The partial specific volume (v-bar) of Sir3p (0.7472 cm^3/g at 20°) was calculated from the primary amino acid sequence, and solvent densities (ρ) were calculated within Ultrascan.

RESULTS

Purification of Recombinant Yeast Sir3p. To obtain quantities of full-length recombinant yeast Sir3p suitable for solution biophysical studies, we scaled up the expression and purification of baculovirus-encoded yeast SIR3 from sf9 cells (*22*). Because of weak binding of the poly-histidine tagged Sir3p to metal-chelate resin, Ni^{2+}-affinity chromatography was omitted from the purification scheme. Instead the 50% ammonium sulfate precipitant was applied sequentially to Q-sepharose FF, Hi-Trap Heparin HP, and Mono Q 5/50 GL columns. Coomassie staining of the purified protein after SDS−PAGE revealed a prominent band at ∼125 kDa (Figure 1A). Western blotting of the same gel using an antibody directed at the C-terminal hexa-histidine tag yielded a major band at ∼125 kDa (data not shown), indicating that ∼125 kDa band was tagged, full-length Sir3p. Samples were routinely >90−95% pure as judged by SDS−PAGE (Figure 1A). The molecular mass of the purified protein was determined by MALDI-TOF mass spectrometry to be 112 301 Da (data not shown), within 1% the molecular weight of 112 182 Da calculated for hexa-histidine tagged Sir3p. To determine if the purified Sir3p was able to bind to nucleosomal arrays, increasing molar ratios of protein were mixed with 12-mer nucleosomal arrays in low-salt TEN buffer, and the samples were electrophoresed on a 1% agarose gel (Figure 1B). Incubation with increasing amounts of Sir3p led to progressive decreases in array mobility, as observed previously (*22*). Thus, the purified full-length Sir3p was functionally competent for chromatin binding.

Sir3p Domain Organization. The per-residue secondary structure content of purified Sir3p was determined using CD spectroscopy. Fitting of the CD spectrum (Figure 2A) obtained under solution conditions of the chromatin binding assay indicated that Sir3p was 31% α-helix, 40% β-sheet/turn, and 29% disordered. The secondary structure content predicted from the amino acid sequence was 31% α-helix, 12% β-sheet/turn, and 57% disordered. Limited trypsin digestion was used to further explore the disorder in Sir3p. Very light digestion conditions (Figure 2B, lanes 8−10) yielded many minor bands, demonstrating that full-length Sir3p was highly sensitive to trypsin proteolysis. Western blotting using an antibody directed at the C-terminal hexa-histidine moiety initially revealed a prominent ∼65 kDa band (Figure 2B, lanes 2−4). More extensive trypsin digestion yielded two protease-resistant bands of ∼48 and ∼23 kDa detected by Coomassie staining (Figure 2B lanes 11−12). Only the 48 kDa band reacted with the anti-hexaHis antibody [as did a minor ∼15 kDa C-terminal fragment not detected by Coomassie (Figure 2B, lanes 5−6)]. These results indicate that the N- and C-terminal regions of Sir3p are digested into stable ∼23 and ∼48 kDa fragments, respectively, and experimentally confirm the large degree of disorder in Sir3p. To help determine the location of the disorder, the Sir3p primary amino acid sequence was analyzed for regions of intrinsic disorder using the FoldIndex algorithm (*29*). A FoldIndex plot of the Sir3p sequence is shown in Figure 2C. A long stretch of negative (red) FoldIndex values is indicative of an intrinsically disordered domain. In contrast, most ordered regions in proteins consist of alternating positive and negative values corresponding to secondary structure motifs and connecting loops, respectively (Hansen, J. C., unpublished). The Sir3p foldIndex plot is complex and can be divided into at least three distinct regions. Residues 45−215 and 550−978 exhibit patterns expected for well-ordered domains, consistent with recent experimental results (*32*−*35*). In contrast, the intervening 335 residues appear largely disordered, including two long stretches (residues 220−275 and 325−475) that are predicted to almost completely lack order. The limited proteolysis, CD, and FoldIndex results are in close agreement, and together indicate that the Sir3p monomer has a tripartite domain organization that includes a long stretch of internal disorder.

Sir3p Quaternary Structure. To determine the oligomeric state of Sir3p under conditions where it binds and condenses chromatin, samples in TEN buffer were characterized by sedimentation velocity. Boundaries were analyzed by the *G*(*s*) method of Demeler and van Holde to obtain an integral distribution of sedimentation coefficients that was corrected for diffusion and is accurate for even highly heterogeneous samples (*30*). A vertical *G*(*s*) plot is indicative of a homogeneous sample, while a heterogeneous sample yields a plot with one or more regions with positive slope. For a protein that is >95% pure, significant slope in the *G*(*s*) plot is diagnostic for the presence of protein oligomers, and the shape of the plot provides insight into the oligomerization

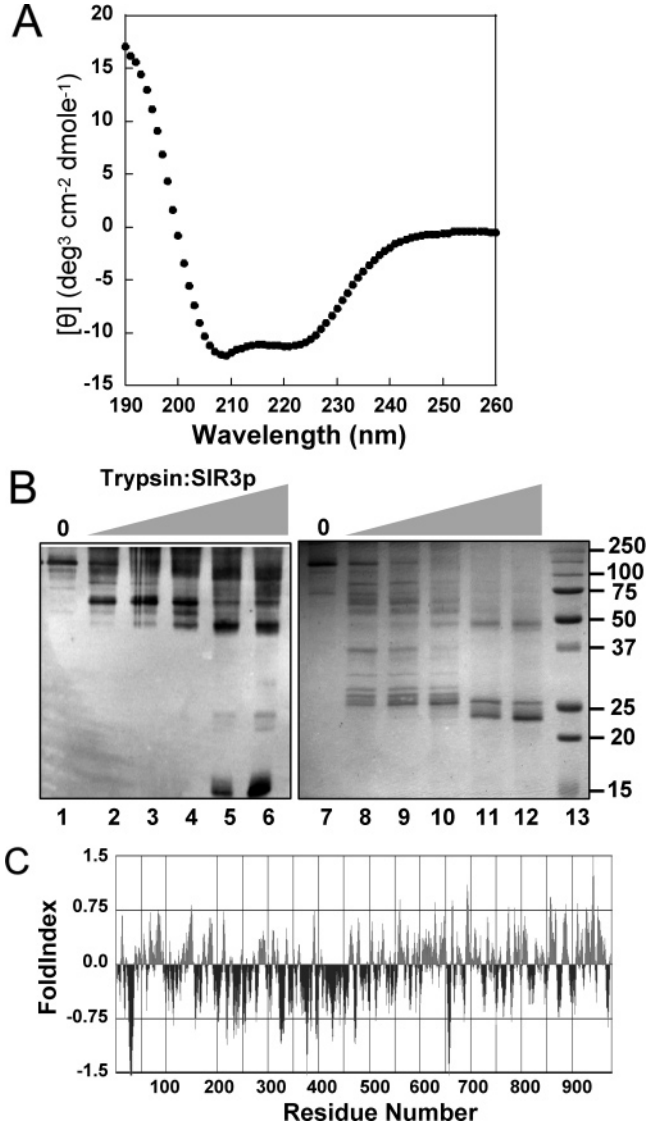

FIGURE 2: Secondary structure analysis of Sir3p: (A) Circular dichroism (CD) spectra were acquired at both 1 and 2 μM Sir3p (the normalized CD spectrum of 1 μM SIR3 protein in 10 mM Tris, pH 7.5, 2 mM NaCl is shown). The two normalized spectra nearly superimposed, confirming the accuracy of the Sir3p concentrations as determined and the validity of the normalized spectrum and resulting analysis. (B) Limited trypsin proteolysis was performed on 10 μg of Sir3p (undigested protein shown in lanes 1 and 7) for 15 min at 22 °C using Sir3p to trypsin ratios (mass: mass) of 2000:1 (lanes 2, 8), 1000:1 (lanes 3, 9), 500:1 (lanes 4,-10), 100:1 (lanes 5 and 11), and 50:1 (lanes 6 and 12). The reactions were quenched by the addition of 0.8% SDS, and the samples were boiled and loaded onto 15% SDS−PAGE gels. The left panel is a Western blot using a monoclonal antibody directed at the carboxyl-terminal, hexa-histidine moiety (lanes 1−6), while the right panel is the Coomassie stain of an identical gel. A protein molecular weight standard (Precision-Plus Dual Color (Bio-Rad)) is shown in lane 13. (C) The FoldIndex prediction for Sir3p. The *y*-axis specifies whether the amino acid (on the *x*-axis) will be contained in an ordered (positive value) or disordered (negative value) state.

process (*36*). At the lowest protein concentration that could be examined with the absorbance optical system (0.56 μM), Sir3p in TEN sedimented as a very heterogeneous mixture of species ranging from 6 to >70 S (Figure 3A). The shape of the $G(s)$ plot was quite distinctive. Approximately 60−70% of the sample sedimented at ~6−13 S. The remainder of the Sir3p spread between ~13 and >70 S, resulting in a pronounced change in slope at ~13 S (Figure 3A; arrow).

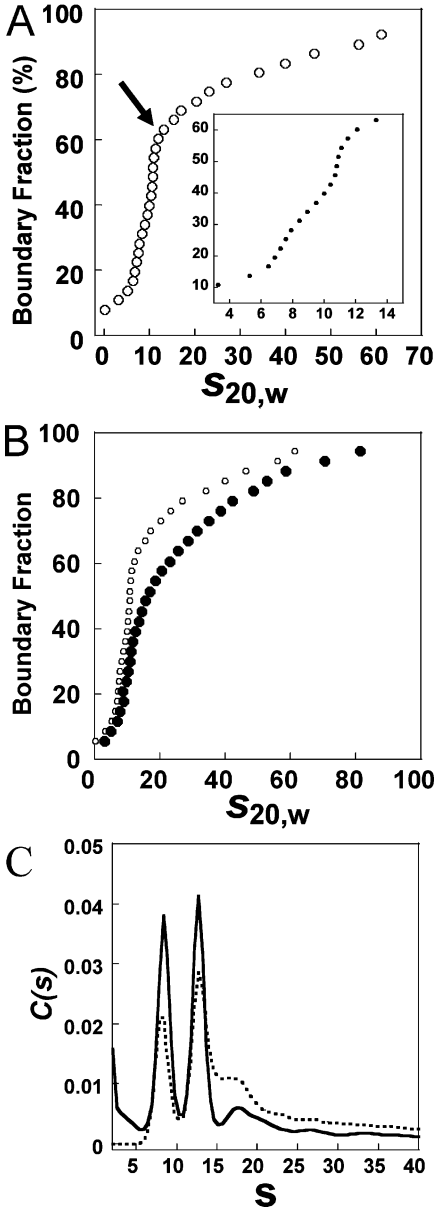

FIGURE 3: Sedimentation velocity of Sir3p. 0.56 μM (○) and 4.8 μM (●) Sir3p were sedimented in 20 mM HEPES, pH 7.5, 2 mM NaCl at 40k rpm in an analytical ultracentrifuge measuring in the absorbance mode at 229 and 276 nm, respectively. In (A) and (B) the boundaries were analyzed using the van Holde-Weischet method and the resulting integral distributions of S ($G(s)$ [corrected for water at 20 °C ($S_{20,w}$)] over the boundary are shown (the data from (A) is also shown in (B) to emphasize the change in the size-distribution with increasing concentration of Sir3p). The inset in (A) expands the 10−65% boundary fraction of (A) to enhance the 6-13S components. In panel (C), the same boundaries as in (A) and (B) were analyzed using Sedfit to return the sedimentation coefficient distribution [$c(S)$].

The inset to Figure 3A shows the 6−13 S region of the plot (boundary fraction = 10−65%) on an expanded scale. The shape is indicative of a multicomponent system consisting of mostly ~8 S, and ~13 S species and very small amounts of a ~6S species. To independently assess the complicated sedimentation velocity boundaries, the same data were analyzed by direct boundary modeling, using finite solutions to the Lamm eq 31. The output of this analysis is a plot of the diffusion-corrected sedimentation coefficient distribution, $c(S)$, in derivative form (Figure 3C, dashed line). There were major peaks in the $c(S)$ plot at ~8 S and ~13 S. A series of

discrete smaller peaks with apparent sedimentation coefficients of approximately 15, 21, 26, and 31 S also were observed (Figure 3A). The results of the *G*(*s*) and *c*(S) analysis methods were internally consistent and indicated that Sir3p oligomerized extensively under the conditions of these experiments.

We next examined Sir3p oligomerization at an 8.5-fold higher protein concentration. *G*(*s*) and *c*(*s*) plots obtained at 4.8 μM Sir3p are shown in Figure 3, panels B and C (solid line), respectively. Relative to the data obtained at 0.56 μM, an 8.5-fold increase in protein concentration increased the fraction of the sample that sedimented at ≥15 S and decreased the fraction of the sample that sedimented at 6−13 S. The ratio of 13 to 8 S species was higher at the higher Sir3p concentration. The largest oligomer detected under these conditions sedimented at ~85 S (Figure 3B). When the 4.8 μM sample was returned to 0.56 μM, the *G*(*s*) plot was identical to that seen originally at the lower concentration (data not shown). These results indicate that Sir3p oligomerization is reversible and mass action driven. The propensity of Sir3p to assemble into large oligomers was also observed during sedimentation equilibrium experiments. The high protein concentrations (>10 μM) generated by the steep concentration gradients led to formation of large oligomers that pelleted during the course of the experiment. This in turn kept the sample from reaching equilibrium and prevented analysis by sedimentation equilibrium.

G(*s*) plots as a function of NaCl concentration are shown in Figure 4A. In 2 mM NaCl, approximately 40% of the Sir3p sample sedimented at >13 S. Less than 25% of Sir3p sedimented at >13 S in 100 and 250 mM NaCl, although significant amounts of the larger oligomers were present under these conditions. Only the 6−13 species were observed in 350−500 mM NaCl, indicating that the higher order Sir3p oligomers were completely dissociated by ≥350 mM salt. The stability of the 8 and 13 S species also was influenced by salt. For example, *c*(*S*) analysis showed that there was more 8 S and less 13 S species in 100 mM NaCl compared 2 mM NaCl, and the 100 mM sample also had a noticeable shoulder at ~6 S (data not shown). In 500 mM NaCl, most of the sample sedimented at 6 S, and only a small amount of 8 S species could be detected. Thus, increasing the salt concentration led to sequential dissociation of Sir3p oligomers and accumulation of a stable 6 S species. The differences in the CD spectra of Sir3p in 2 and 500 mM NaCl were small but reproducible (Figure 4B), suggesting that oligomerization was accompanied by a subtle change in secondary structure. We also observed that a fraction of the Sir3p sample formed pelletable aggregates in 50−200 mM NaCl (Figure 4C).

To distinguish whether the stable ~6S species identified in Figures 2−5 was a monomer or dimer, sedimentation velocity and CD experiments were performed in the presence of guanidine hydrochloride (GuHCl). Sir3p oligomerization was highly sensitive to this chaotrope; addition of only 0.25 M GuHCl was sufficient to convert the highly heterogeneous Sir3p sample seen under native conditions into a nearly homogeneous sample in which 70−75% of the Sir3p sedimented at ~6 S (Figure 5A). The CD spectrum in 0.25 M GuHCl closely resembled that seen in TEN, indicating that the ~6 S species retained most of its native secondary structure under these conditions (Figure 5B). In contrast, in

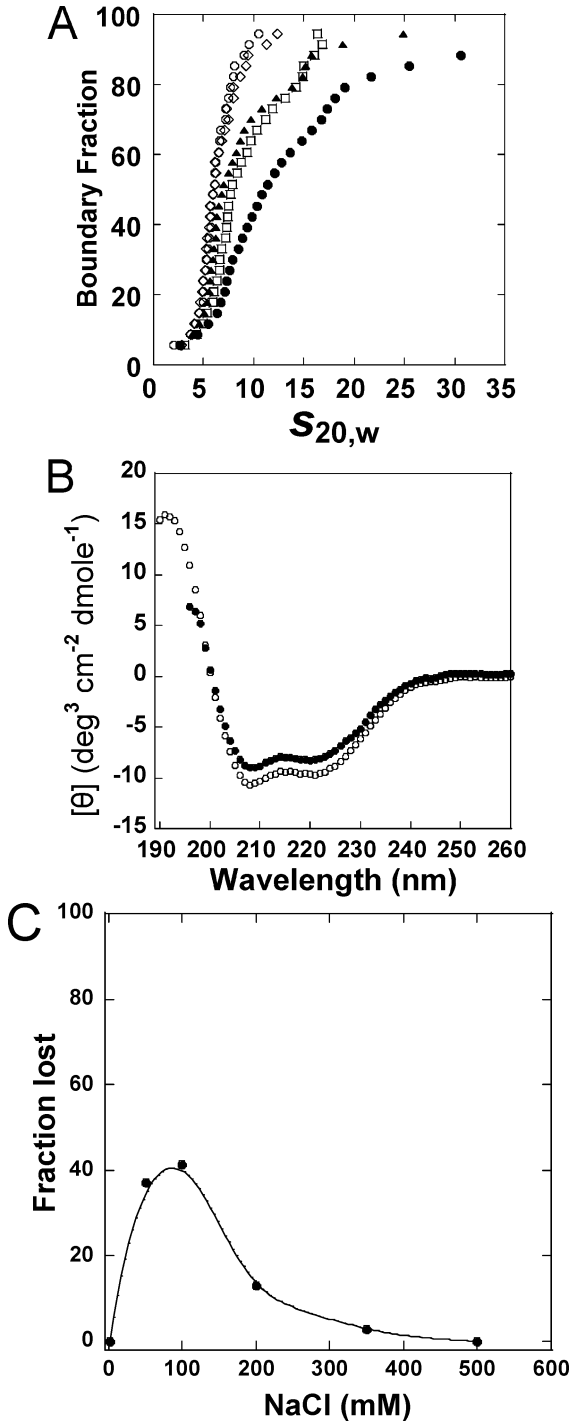

FIGURE 4: The affect of NaCl on Sir3p self-association. (A) Identical concentrations of Sir3p (0.66 μM) were sedimented at 2 mM NaCl (●), 100 mM NaCl (□), 250 mM NaCl (▲), 350 mM NaCl (◇), and 500 mM NaCl (○). The boundaries were analyzed as described in M&M, and the resulting integral distributions of S over the boundary are shown. (B) CD spectra of identical concentrations of Sir3p (1 μM) at 500 mM (●) NaCl and 2 mM NaCl (○). Data collection was terminated at 195 nm for the 500 mM NaCl sample due to high absorbance in the far UV. (C) The fraction (based on measured absorbance) of total Sir3p which pelleted during sedimentation velocity in (A) was plotted as a function of the NaCl concentration. Data from NaCl concentrations not shown in (A) are included, and a smooth curve of the data points is shown.

1 M GuHCl most of the Sir3p sedimented at ~5 S, and there was a significant loss of secondary structure as indicated by the large decrease in intensity at 222 nm in the CD spectrum.

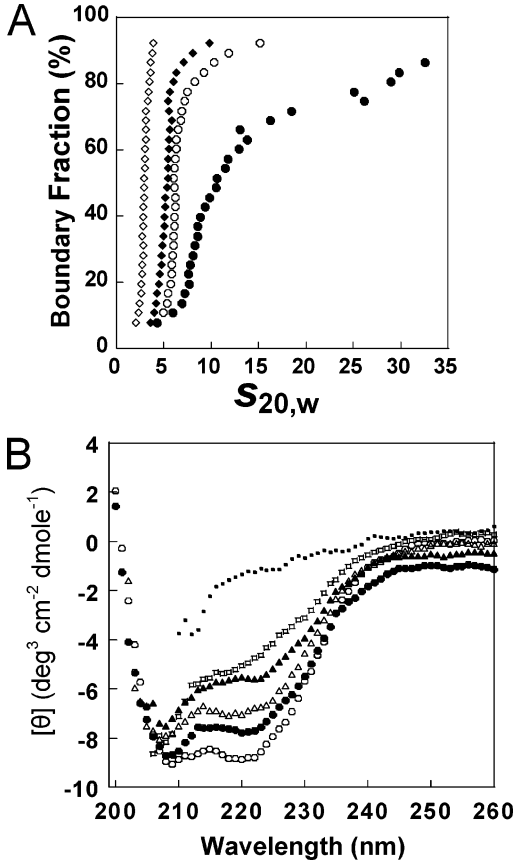

FIGURE 5: Sedimentation velocity and CD spectroscopy of Sir3 in the presence of guanidine hydrochloride (GuHCl). (A) Equivalent concentrations of Sir3p (3.9 μM) were sedimented in the presence of 0 (●), 0.25 (○), 1.0 (◆), and 6 M GuHCl (◇) and the resulting integral distribution of S (corrected for water at 20 C) over the boundary is shown. (B) CD spectroscopy was performed on 1 μM Sir3p in the presence of 0 M (○), 0.25 M (●), 0.5 M (△), 1 M (▲), 2 M (□), and 4 M (■) guanidine hydrochloride. The spectra were analyzed as described in M&M.

In 6 M GuHCl, all of the Sir3p sedimented at ~3−4 S and the CD spectrum was characteristic of a denatured protein. Using dimethyl suberimidate, we observed that the fraction of ~120 kDa monomer seen by SDS−PAGE after cross-linking increased in 350 mM NaCl (data not shown), concomitant with the increase in 6 S species seen in sedimentation velocity experiments (Figure 5A). From these results, we conclude that the ~6 S species is the native Sir3p monomer.

DISCUSSION

Physicochemical characterization of full-length recombinant Sir3p has provided insight into the domain organization and quaternary structure of this chromatin architectural protein. The Sir3p monomer contains a long stretch of intrinsic disorder located between its structured N- and C-terminal regions, resulting in a unique multidomain protein with a large number of macromolecular interaction interfaces (Figure 6). Digestion of Sir3p with trypsin identified two protease-resistant domains, an N-terminal ~23 kDa fragment and a C-terminal ~48 kDa fragment. The N-terminal fragment likely corresponds to the recently crystallized (*33*, *34*) BAH domain (residues 1−215). We believe that the ~48 kDa C-terminal Sir3p fragment includes residues 550−980. This region is predicted to be well ordered (Figure 2C) and

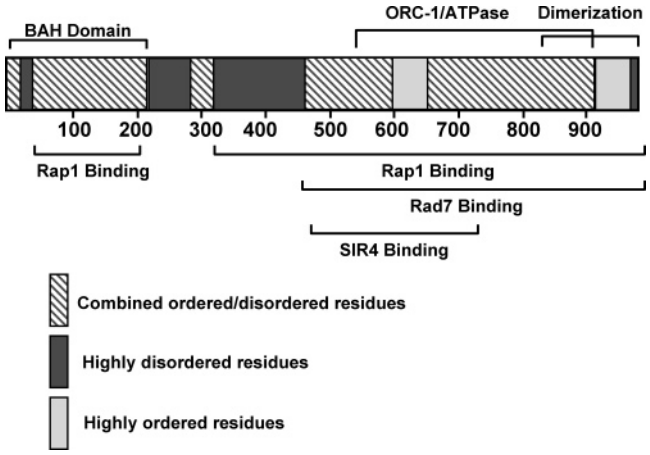

FIGURE 6: Multiple interaction domains exclusively overlay the structured regions of Sir3p. The characterized interaction domains primarily reside in the ordered C-terminal half of the protein (*32*, *35*, *37*, *38*, *41*). Highly ordered residues are denoted by gray boxes, while alternating order and disorder is denoted by striped boxes (as predicted by FoldIndex). These interaction surfaces do not generally include the intrinsically disordered regions (denoted by dark boxes). The structured, N-terminal BAH domain (*33*, *34*) is co-incident with residues that have been experimentally shown, as well as predicted by FoldIndex, to be well ordered.

contains binding sites for RAP1p (*37*, *38*), the histone H3 and H4 N-terminal domains (*39*, *40*), and RAD7p (*41*). This region also plays a key role in Sir3p dimerization (*35*; see below). A major finding of our work is that the structured Sir3p N- and C-terminal domains are connected by a very long stretch of amino acids (~335 residues) that is protease-sensitive and predicted to be mostly intrinsically disordered (ID). CD studies demonstrated that over 30% of the Sir3p sequence is unstructured, while protease digestion data (Figure 2C; *32*) and FoldIndex plots (Figure 2D) suggest that most of the disorder lies between residues ~215−550. These boundaries are consistent with crystallographic (*33*, *34*) and protease digestion (*35*) studies of C- and N-terminal SIR3p fragments, respectively. The internal disordered region is noticeably deficient in hydrophobic residues, another characteristic of an ID domain. ID regions often function as binding interfaces that become structured through a process that couples binding and protein folding (*42*−*45*). The internal Sir3p ID region has been implicated in binding to RAP1p (*37*, *38*) and RAD7p (*41*), and disordered residues 495−521 are critical for binding to the Sir4p coiled-coil domain (*32*). We note that there are many small "islands" of order predicted to lie within the internally disordered region (Figure 2C) and that the 6 S Sir3p monomer has a more spherical shape ($f/f_o \cong 1.5$) than would be expected if residues 215−550 were fully extended. Thus, the ID region within the Sir3p monomer may assume specific structural motifs in response to Sir3p interacting with itself and (or) other macromolecules. This conclusion is further supported by the finding that dissociation of Sir3p oligomers leads to an increase in the CD signal at 222 nm (Figure 4B), Also, the measured disorder within Sir3p when oligomeric (29%, Figure 2A) is much less than predicted from the amino acid sequence (57%). While more work will be needed to decipher the role of intrinsic disorder in Sir3p action, the presence of a large internal ID region significantly impacts how one envisions the structure and function of the full-length protein.

Our results demonstrate that Sir3p populates an unusually wide range of oligomeric states in moderate salt and at micromolar protein concentrations in vitro. Although this complexity prevented characterization by sedimentation equilibrium, sedimentation velocity studies allowed us to identify the components of the self-association pathway and determine how the stabilities of different Sir3p oligomers are influenced by salt and chaotrope. Sir3p oligomerization can be portrayed in hydrodynamic terms as a 6 S ↔ 8 S ↔ 13 S ↔ [>13 S] equilibrium. The 6 S species is the tripartite monomer discussed above. The 8 and 13 S species most likely equate to Sir3p dimers and tetramers, respectively. Ellenberger and colleagues have shown that the C-terminal Sir3p domain (residues 464−972) forms an antiparallel dimer (*32*, *35*). Arrangement of two full-length Sir3p monomers (6 S; $f/f_o \cong 1.5$) in the same antiparallel fashion is predicted to yield a ~8 S dimer with an $f/f_o \cong 1.7$. In contrast, the predicted f/f_o of an 8 S trimer is well above 2.0 and would require a head to tail-like association mechanism. Similarly, the 13 S species is well modeled as a tetramer of two 8 S dimers, while it is difficult to form a 13 S trimer from an antiparallel 8 S dimer. The [>13 S] term describes a population of defined higher order oligomers that are assembled from (and dissociate into) the 8 and 13 S species (Figures 2−5) and have sedimentation coefficients ranging from 16 to 85 S. The assembly of higher order Sir3p oligomers is open-ended, i.e., an upper size limit could not be detected. There was very little 6 S monomer (<5%) present at 0.56 μM Sir3p, while an increase to 4.4 μM shifted the equilibrium toward the 13 S species and higher order oligomers (Figure 2). Thus, the apparent K_d for Sir3p dimerization approaches nanomolar, while the K_d for formation of all other Sir3p oligomers is closer to micromolar. The lesser stability of the higher order oligomers is further evidenced by their increased susceptibility to dissociation by high salt and GnHCl. Liou et al. (*5*) recently concluded from sedimentation velocity and cross-linking data that affinity purified *S. cerevisiae* Sir3p also exists in dimeric, tetrameric, and higher order states, although the sedimentation coefficients derived for the monomer, dimer, and tetramer (3, 5, and 7 S, respectively) are too low for a 113 kDa protein and better support a monomer−dimer model. Nevertheless, all available evidence is consistent with an oligomerization mechanism in which stable Sir3p dimers reversibly associate into tetramers and a wide range of higher order oligomers under physiological solution conditions.

Sir3p is structurally related to ORC1p, one of six subunits of the heteromeric ORC (*46*−*48*). Whereas ORC1 is found in all fungal genomes, Sir3p is only found in the *Saccharomyces* branch. It has recently been shown that the *S. cerevisiae Sir3* gene evolved from one of the duplicated *Orc1* genes generated by a whole genome duplication event (WGDE) in the common ancestor to *S. cerevisiae* and *Candida glabrata* (*49*). Importantly, homologs of known Sir3p binding partners such as Sir2p, SIR4, and RAP1p were present in genome of the duplicated ancestor, although Sir3p itself was not (*49*). Hence, it appears that the evolution of Sir3p and its unique structural properties in the period after the WGDE was the defining event in the evolution of transcriptional silencing in the *Saccharomyces* lineage. This in turn implies that the complicated Sir3p oligomerization pathway characterized in our studies evolved for a specific functional purpose. The ability of Sir3p to extensively oligomerize is likely to be directly related to the degree of genome compaction in silenced chromatin regions and the ability of silenced chromatin to spread into euchromatic regions. Sir3p can bind to both DNA (*22*) and the histone H3 and H4 NTDs (*5*, *21*, *22*, *39*, *40*), and presumably these properties reside in each Sir3p monomer. Thus, Sir3p oligomers will be multivalent for chromatin, and conditions that promote Sir3p oligomerization will lead to a greater degree of nucleosome−nucleosome bridging. This in turn can result in either a more densely compacted genomic region or an increase in the size of the silenced region, i.e., spreading. We have tested this model by studying the architectural consequences of Sir3p−nucleosomal array interactions. In electron microscopy experiments, we have directly visualized Sir3p-dependent nucleosome−nucleosome bridging in both cis and trans. These interactions lead to local and global conformational changes, ultimately yielding highly condensed, structurally complex assemblages containing many nucleosomal arrays. The observed dependence of chromatin condensation on SIR3p concentration is consistent with a role for SIR3p oligomers in spreading of silent chromatin (McBryant, et al., manuscript in preparation).

REFERENCES

1. Rusche, L. N., Kirchmaier, A. L., and Rine, J. (2003) The establishment, inheritance, and function of silenced chromatin in *Saccharomyces cerevisiae*, *Annu. Rev. Biochem. 72*, 481−516.
2. Chien, C. T., Buck, S., Sternglanz, R., and Shore, D. (1993) Targeting of SIR1 protein establishes transcriptional silencing at HM loci and telomeres in yeast, *Cell 75*, 531−541.
3. Triolo, T., and Sterngalanz, R. (1996) Role of interactions between the origin recognition complex and SIR1 in transcriptional silencing, *Nature 381*, 251−2533.
4. Gardner, K. A., Rine, J., and Fox, C. A. (1999) A region of the Sir1 protein dedicated to recognition of a silencer and required for interaction with the Orc1 protein in Saccharomyces cerevisiae, *Genetics 151*, 31−44.
5. Liou, G. G., Tanny, J. C., Kruger, R. G., Walz, T., and Moazed, D. (2005) Assembly of the SIR complex and its regulation by O-acetyl-ADP-ribose, a product of NAD-dependent histone deacetylation, *Cell 121*, 515−527.
6. Fox, C. A., and McConnell, K. H. (2005) Toward biochemical understanding of a transcriptionally silenced chromosomal domain in Saccharomyces cerevisiae, *J. Biol. Chem. 280*, 8629−8632.
7. Rudner, A. D., Hall, B. E., Ellenberger, T., and Moazed, D. (2005) A nonhistone protein-protein interaction required for assembly of the SIR complex and silent chromatin, *Mol. Cell. Biol. 11*, 4514−4528.
8. Hoppe, G. J., Tanny, J. C., Rudner, A. D., Gerber, S. A., Danaie, S., Gygi, S. P., and Moazed, D. (2002) Steps in assembly of silent chromatin in yeast: Sir3-independent binding of a Sir2/Sir4 complex to silencers and role for Sir2-dependent deacetylation, *Mol. Cell. Biol. 22*, 4167−4180.
9. Moazed, D., Kistler, A., Axelrod, A., Rine, J., and Johnson, A. D. (1997) Silent information regulator protein complexes in *Saccharomyces cerevisiae*: A SIR2/SIR4 complex and evidence for a regulatory domain in SIR4 that inhibits its interaction with SIR3, *Proc. Natl. Acad. Sci. U.S.A. 94*, 2186−2191.
10. Fogel, S., Klar, A. J. S., and MacLeod, K. (1979) MAR1 {sir2} − a regulator of the HMa and HMα loci in Saccharomyces cerevisiae, *Genetics 93*, 37−50.
11. Klar, A. J. (1980) Interconversion of yeast cell types by transposable genes, *Genetics 95*, 631−648.
12. Feldman., J. B., Hicks, J. B., and Broach, J. R. (1984) Identification of sites required for repression of a silent mating type locus in yeast, *J. Mol. Biol. 178*, 815−834.
13. Gardner, K. A., and Fox, C. A. (2001) The Sir1 protein's association with a silenced chromosome domain, *Genes Dev. 15*, 147−157.

14. Fox., C. A., Ehrenhofer-Murray, A. E., Loo, S., and Rine, J. (1997) The origin recognition complex, SIR1, and the S phase requirement for silencing, *Science 276*, 1547−1551.
15. Rusche, L. N., Kirchmaier, A. L., and Rine, J. (2002) Ordered nucleation and spreading of silenced chromatin in Saccharomyces cerevisiae, *Mol. Biol. Cell. 7*, 2207−2222.
16. Zhang, A., Hayashi, M. K., Merkel, O., Stillman, B., and Xu, R. M. (2002) Structure and function of the BAH-containing domain of Orc1p in epigenetic silencing, *EMBO J. 21*, 4600−4611.
17. Ghidelli, S., Donze, D., Dhillon, N., and Kamakaka, R. T. (2001) Sir2p exists in two nucleosome-binding complexes with distinct deacetylase activities, *EMBO J. 20*, 4522−4535.
18. Imai, S., Armstrong, C. M., Kaeberlein, M., and Guarente, L. (2000) Transcriptional silencing and longevity protein Sir2 is an NAD-dependent histone deacetylase, *Nature 403*, 795−800.
19. Tanny, J. C., and Moazed, D. (2001) Coupling of histone deacetylation to NAD breakdown by the yeast silencing protein Sir2: Evidence for acetyl transfer from substrate to an NAD breakdown product, *Proc. Natl. Acad. Sci. U.S.A. 98*, 415−420.
20. Suka, N., Suka, Y., Carmen, A. A., Wu, J., and Grunstein M. (2001) Highly specific antibodies determine histone acetylation site usage in yeast heterochromatin and euchromatin, *Mol. Cell. 2*, 473−479.
21. Carmen, A. A., Milne, L., and Grunstein, M. (2002) Acetylation of the yeast histone H4 N terminus regulates its binding to heterochromatin protein SIR3, *J. Biol. Chem. 277*, 4778−4781.
22. Georgel, P. T., Palacios DeBeer, M. A., Pietz, G., Fox, C. A., and Hansen, J. C. (2001) Sir3-dependent assembly of supramolecular chromatin structures *in vitro*, *Proc. Natl. Acad. Sci. U.S.A. 98*, 8584−8589.
23. McBryant, S. J., Adams, V. H., and Hansen, J. C. (2006) Chromatin architectural proteins, *Chromosome Res. 14*, 39−51.
24. Hecht, A., Strahl-Bolsinger, S., and Grunstein, M. (1996) Spreading of transcriptional repressor SIR3 from telomeric heterochromatin, *Nature 383*, 92−96.
25. Renuald, H., Aparicio, O. M., Zierath, P. D., Billington, B. L., Chhablani, S. K., and Gottschling, D. E. (1993) Silent domains are assembled continuously from the telomere and are defined by promoter distance and strength, and by SIR3 dosage, *Genes Dev. 7A*, 1133−1145.
26. Strahl-Bolsinger, S., Hecht, A., Luo, K., and Grunstein, M. (1997) SIR2 and SIR4 interactions differ in core and extended telomeric heterochromatin in yeast, *Genes Dev. 11*, 83−93.
27. Hansen, J. C., and Lohr, D. (1993) Assembly and structural properties of subsaturated chromatin arrays, *J. Biol. Chem. 268*, 5840−5848.
28. Sreerama, N., and Woody, R. W. (2000) Estimation of protein secondary structure from circular dichroism spectra: comparison of CONTIN, SELCON, and CDSSTR methods with an expanded reference set, *Anal. Biochem. 287*, 252−260.
29. Prilusky, J., Felder, C. E., Zeev-Ben-Mordehai, T., Rydberg, E. H., Man, O., Beckmann, J. S., Silman, I., and Sussman, J. L. (2005) FoldIndex: a simple tool to predict whether a given protein sequence is intrinsically unfolded, *Bioinformatics 21*, 3435−3438.
30. Demeler, B., and van Holde, K. E. (2004) Sedimentation velocity analysis of highly heterogeneous systems, *Anal. Biochem. 335*, 279−288.
31. Schuck, P. (2000) Size-distribution analysis of macromolecules by sedimentation velocity ultracentrifugation and lamm equation modeling, *Biophys. J. 78*, 1606−1619.
32. Chang, J. F., Hall, B. E., Tanny, J. C., Moazed, D., Filman, D., and Ellenberger, T. (2003) Structure of the coiled-coil dimerization motif of Sir4 and its interaction with Sir3, *Structure 11*, 637−649.
33. Connelly, J. J., Yuan, P., Hsu, H. C., Li, Z., Xu, R. M., and Sternglanz, R. (2006) Structure and function of the Saccharomyces cerevisiae Sir3 BAH domain, *Mol. Cell. Biol. 26*, 3256−3265.
34. Hou, Z., Danzer, J. R., Fox, C. A., and Keck, J. L. (2006) Structure of the Sir3 protein bromo adjacent homology (BAH) domain from S. cerevisiae at 1.95 A resolution, *Protein Sci. 15*, 1182−1186.
35. King, D. A., Hall, B. E., Iwamoto, M. A., Win, K. Z., Chang, J. F., and Ellenberger, T. (2006) Domain structure and protein interactions of the silent information regulator sir3 revealed by screening a nested deletion library of protein fragments, *J. Biol. Chem. 281*, 20107−20119.
36. Demeler, B., Saber, H., and Hansen, J. C. (1997) Identification and interpretation of complexity in sedimentation velocity boundaries, *Biophys. J. 72*, 397−407.
37. Moretti, P., Freeman, K., Coodly, L., and Shore, D. (1994) Evidence that a complex of SIR proteins interacts with the silencer and telomere-binding protein RAP1, *Genes Dev. 8*, 2257−2269.
38. Liu, C., and Lustig, A. J. (1996) Genetic analysis of Rap1p/Sir3p interactions in telomeric and HML silencing in Saccharomyces cerevisiae, *Genetics 143*, 81−93.
39. Johnson, L. M., Kayne, P. S., Kahn, E. S., and Grunstein, M. (1990) Genetic evidence for an interaction between SIR3 and histone H4 in the repression of the silent mating loci in Saccharomyces cerevisiae, *Proc. Natl. Acad. Sci. U.S.A. 87*, 6286−6290.
40. Hecht, A., Laroche, T., Strahl-Bolsinger, S., Gasser, S. M., and Grunstein, M. (1995) Histone H3 and H4 N-termini interact with SIR3 and SIR4 proteins: a molecular model for the formation of heterochromatin in yeast, *Cell 80*, 583−592.
41. Paetkau, D. W., Riese, J. A., MacMorran, W. S., Woods, R. A., and Gietz, R. D. (1994) Interaction of the yeast RAD7 and SIR3 proteins: implications for DNA repair and chromatin structure, *Genes Dev. 1994. 8*, 2035−2045.
42. Uversky, V. N., Oldfield, C. J., and Dunker, A. K. (2005) Showing your ID: intrinsic disorder as an ID for recognition, regulation and cell signaling, *J. Mol. Recognit. 18*, 343−384.
43. Tompa, P., Dosztanyi, Z., and Simon, I. (2006) Prevalent Structural Disorder in *E. coli* and *S. cerevisiae* Proteomes, *J. Proteome Res. 8*, 1996−2000.
44. Dyson, H. J., and Wright, P. E. (2005) Intrinsically unstructured proteins and their functions, *Nat. Rev. Mol. Cell. Biol. 6*, 197−208.
45. Hansen, J. C., Lu, X., Ross, E. D., and Woody, R. W. (2006) Intrinsic protein disorder, amino acid composition, and histone terminal domains, *J. Biol. Chem. 281*, 1853−1856.
46. DePamphilis, M. L. (2005) Cell cycle dependent regulation of the origin recognition complex, *Cell Cycle 4*, 70−79.
47. Stone, E. M., and Pillus, L. (1988) Silent chromatin in yeast: an orchestrated medley featuring Sir3p, *Bioessays 20*, 30−40.
48. Cvetic, C., and Walter, J. C. (2005) Eukaryotic origins of DNA replication: could you please be more specific? *Semin. Cell Dev. Biol. 16*, 343−353.
49. Dietrich, F. S., Voegeli, S., Brachat, S., Lerch, A., Gates, K., Steiner, S., Mohr, C., Pohlmann, R., Luedi, P., Choi, S., Wing, R. A., Flavier, A., Gaffney, T. D., and Philippsen, P. (2004) The *Ashbya gossypii* genome as a tool for mapping the ancient *Saccharomyces cerevisiae* genome, *Science 304*, 304−307.

BI061693K